Drag enhancement and drag reduction in viscoelastic fluid flow around a cylinder

2010 EPL 91 64001

(http://iopscience.iop.org/0295-5075/91/6/64001)

A Letters Journal Exploring the Frontiers of Physics

September 2010

EPL, **91** (2010) 64001
doi: 10.1209/0295-5075/91/64001

www.epljournal.org

Drag enhancement and drag reduction in viscoelastic fluid flow around a cylinder

Y. L. Xiong[1], C. H. Bruneau[1] and H. Kellay[2]

[1] *Université Bordeaux 1, Institut de Mathématiques de Bordeaux, INRIA Team MC2, CNRS UMR 5251 351 cours de la Libération, 33405 Talence, France, EU*
[2] *Université Bordeaux 1, Centre de Physique Moléculaire Optique et Hertzienne, UMR 5798 CNRS 351 cours de la Libération, 33405 Talence, France, EU*

received 16 June 2010; accepted in final form 8 September 2010
published online 14 October 2010

PACS 47.20.Gv – Viscous and viscoelastic instabilities
PACS 47.27.ek – Direct numerical simulations
PACS 47.27.nd – Channel flow

Abstract – We here use direct numerical simulations to describe the flow of a viscoelastic fluid, modeled using the so-called Oldroyd B model, around a cylinder in two dimensions. A wide range of flow parameters is covered in these simulations allowing to draw definitive conclusions as to the effect of viscoelasticity on such a flow situation. Both drag enhancement and drag reduction are observed and a phase diagram is proposed in the parameter space Reynolds number *vs.* Weissenberg number. While only drag enhancement is observed below a Reynolds number of 40, both drag enhancement and drag reduction are observed for higher Reynolds numbers indicating that drag reduction is a feature associated with the shedding of vortices behind the cylinder. An interesting observation accompanies the onset of drag enhancement in the vortex-shedding regime: the shedding is suppressed.

One of the most important problems in non-Newtonian fluid mechanics is drag reduction. This peculiar flow feature common to a variety of complex fluids is perhaps the most useful ingredient for transporting fluids over large distances at a reduced cost and for minimizing losses for flows in the presence of obstacles [1]. Several applications have ensued following the discovery of the drag-reducing ability of several fluids, especially polymer solutions and surfactant solutions. Many attempts at understanding this phenomenon have brought the subject to a relatively mature state with different proposed mechanisms such as the ability of polymers to modify the boundary layer flow or their ability to stretch in a variety of flows [2–4]. Still the issue is far from being completely understood and experiments as well as numerical simulations are used routinely to shed light on the problem.

A now standard situation to understand flows of complex fluids, and notably those giving rise to drag reduction, is flow past a cylinder [5]. Let us recall that such a situation is widely studied, experimentally, for low Reynolds numbers where important drag enhancement has been observed and documented for different fluids [6–8]. Simulations have addressed the issue and observations of such enhancement have been reported [9–12]. A complication with some of the experiments is the presence of shear-thinning effects which may influence the drag. Experiments with Boger fluids [8,13] minimize such effects. For high Reynolds numbers, few experiments have been carried out in two-dimensional systems but the modification of the vortex street behind a cylinder [14] and turbulent drag reduction have been reported both experimentally for an array of cylinders and numerically [15,16]. An important question is how does the drag on a cylinder vary in the parameter space described by the two dimensionless numbers namely the Weissenberg number and the Reynolds number.

We here study the simple case of flow around a cylinder of a viscoelastic fluid in two dimensions using direct numerical simulations to cover a wide range in both the Reynolds number Re and the Weissenberg number Wi which measures the ability of the fluid to change properties with respect to external stresses. To our knowledge this is the most comprehensive study to date. We measure the drag on the cylinder and show that this simple flow situation presents a non-trivial transition from drag enhancement to drag reduction. A full phase diagram in

the parameter space *Re*-*Wi* extending for 5 decades in Reynolds number is presented showing the extent of the different regimes. Attention is then brought to the stresses, pressure, elongation, and shear distributions in the flow domain.

The dynamics of an incompressible two-dimensional viscoelastic Oldroyd-B constitutive fluid is described by the following non-dimensional equations which are penalized to represent the solid body on a Cartesian mesh of the domain whose length is 4 times its width:

$$\boldsymbol{\nabla}\cdot\mathbf{u}=0,$$
$$\partial_t\mathbf{u}+(\mathbf{u}\cdot\boldsymbol{\nabla})\mathbf{u}+\frac{\mathbf{u}}{K}=-\boldsymbol{\nabla}p+\frac{1}{Re}[(1-\epsilon)\Delta\mathbf{u}+\frac{\epsilon}{Wi}\boldsymbol{\nabla}\cdot\boldsymbol{\sigma}],$$
$$\partial_t\boldsymbol{\sigma}+(\mathbf{u}\cdot\boldsymbol{\nabla})\boldsymbol{\sigma}+\frac{\boldsymbol{\sigma}}{K}+\frac{\boldsymbol{\sigma}-\mathbf{I}}{Wi}=(\boldsymbol{\nabla}\mathbf{u})\cdot\boldsymbol{\sigma}+\boldsymbol{\sigma}\cdot(\boldsymbol{\nabla}\mathbf{u})^T+\kappa\Delta\boldsymbol{\sigma},$$

where $\mathbf{u}$ is the two-dimensional velocity vector, p is the pressure, σ is the conformation tensor of polymer molecules, their elongation is measured by its trace; K is the non-dimensional permeability coefficient used in the penalization term. It is set to 10^{16} in the fluid zone to recover the genuine equations and to 10^{-7} in the solid cylinder to enforce $\mathbf{u}$ and σ to vanish [17]. The quantity $(1-\epsilon)$ denotes the ratio of the solvent viscosity to the viscosity of polymer solution, it is 0.99 in our simulations. The term $\kappa\Delta\sigma$ is an artificial diffusive term to prevent numerical instabilities [18]. The Reynolds number Re and the Weissenberg number Wi are non-dimensionalized by the same referenced velocity and length. In our results, the Drag coefficient Cd is defined by $F/\rho U^2 R$, Re and Wi are defined by $Re=2UR/\eta$ and $Wi=\tau U/R$, respectively, where U is the mean velocity of the inlet Poiseuille flow, $R=0.05$ is the radius of the cylinder located at $(1,0.5)$ (*i.e.* in the middle of the channel at one width from the entrance), F is the drag force on the cylinder, η and τ are, respectively, the viscosity and the relaxation time of the polymer solutions. The numerical simulations are carried out by a multigrid method with a 2048×512 fine grid and a finite-differences approximation [19]. This numerical scheme has been shown to give excellent agreement with experimental measurements of two-dimensional flows in the turbulent state [20]. It should be noted that the choice of the Oldroyd-B model is dictated by its simplicity despite the fact that it has limitations [21]. This model has also been shown to display several features observed in experiments such as drag reduction and elastic turbulence [16].

Our main result is illustrated in fig. 1 which shows a phase diagram of the different regimes observed in the parameter space *Re*-*Wi*. This graph shows that three regions can be identified for the behavior of the drag on the cylinder: A Newtonian regime for low Wi, a drag enhancement regime for high Wi, and a drag-reducing regime for intermediate Wi. This drag reduction regime exists only for Re greater than 40. Indeed, for $Re\leqslant 40$,

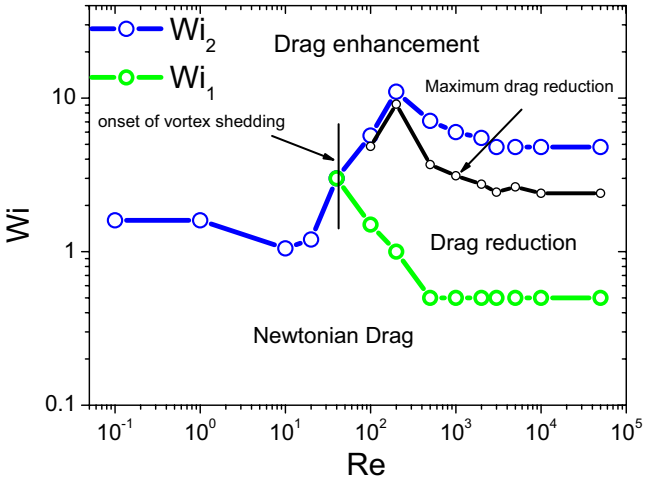

Fig. 1: (Colour on-line) Phase Diagram in *Re*-*Wi* space indicating the drag enhancement and drag reduction regimes. The solid line connecting the small circles indicates the locatin of maximum drag reduction.

only two regimes are observed: either the fluid is acting as its Newtonian counterpart for small values of Wi below a threshold Wi_2 or the fluid shows enhanced drag on the cylinder for $Wi>Wi_2$. For $Re>40$, three different regions are observed. Below a first threshold value which we call Wi_1, the fluid behaves as a Newtonian fluid. For intermediate values between Wi_1 and Wi_2, drag reduction is obtained. Above Wi_2, only drag enhancement is observed. This diagram, which spans roughly 5 decades in Reynolds number, summarizes our findings and shows that both drag enhancement and drag reduction can be obtained but only for specific parts of the parameter space. To our knowledge, no such insight into both drag reduction and drag enhancement has been brought forth before and our results show that both phenomena can be related in a full-parameter space representation. Both drag reduction and drag enhancement are present in our simulations but in different regions of the phase diagram. The phase diagram of this behavior is an important result which, though it has been shown before for particular values of the Reynolds number, has not been put forth in such a systematic manner. In addition to these considerations, the maximum drag reduction turns out to be near 50% and is practically independent of the Reynolds number in the asymptotic large Re limit. It should be noted here that the transition from drag enhancement to both drag reduction and drag enhancement occurs at a value of the Reynolds number close to $Re=40$, which coincides with the transition to the vortex-shedding regime for the wake behind the cylinder pointing to a strong dependence on the structure of the flow and to the presence of vortices. Other interesting features emerge such as the suppression of the vortex shedding in the drag enhancement regime.

Figure 2 displays the main flow features observed in this study: The vorticity contour plots are shown for

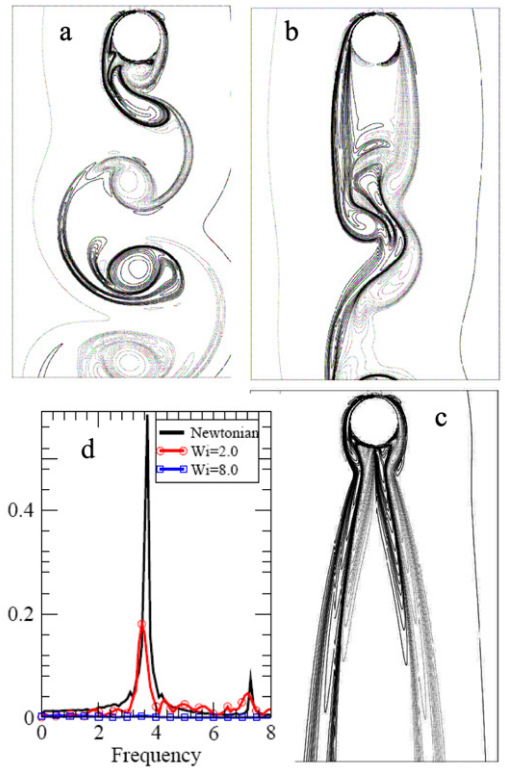

Fig. 2: (Colour on-line) Flow structure around a cylinder for $Re = 1000$ and different Wi (a: $Wi = 0$, b: $Wi = 2$, c: $Wi = 6$). d: spectrum of the transverse component of the velocity for different Wi.

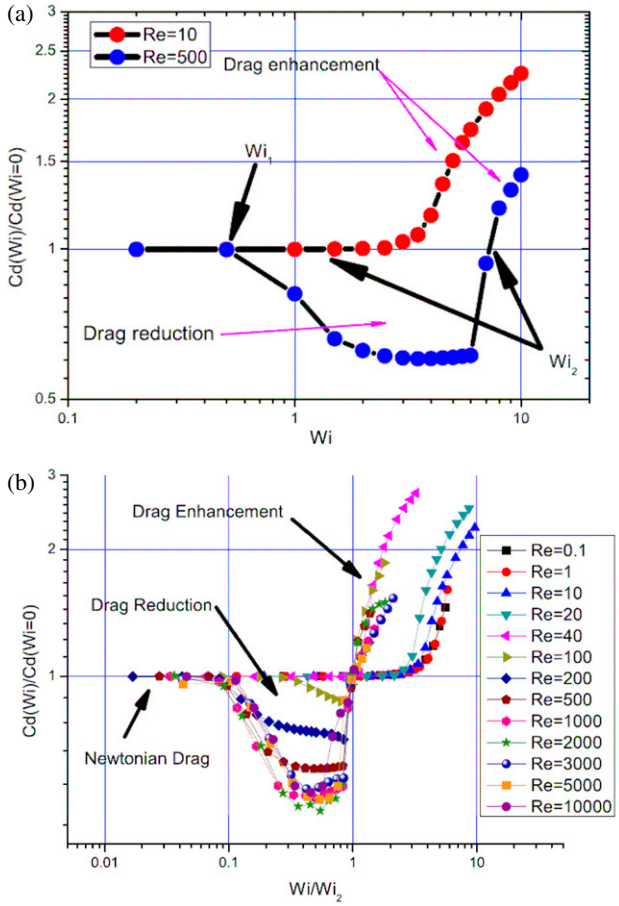

Fig. 3: (Colour on-line) a) Drag on the cylinder, normalized by the Newtonian drag, *vs.* Wi for two different Re. Note the drag enhancement at low Re and both drag enhancement and drag reduction for the higher Re. b) normalized drag *vs.* reduced Wi for different Re.

a Reynolds number of 1000 and different Weissenberg numbers. Perhaps the most striking observation is the disappearance of vortex shedding behind the cylinder for high Weissenberg numbers. For $Re > 40$ (vortex shedding sets in in our simulations in accordance with previous observations) and for Wi greater than Wi_2, vortex shedding is inhibited in our simulations as shown in fig. 2. When drag enhancement is observed the structure of the flow behind the cylinder in the vortex-shedding regime is completely inhibited indicating a strong coupling between the flow structure and the viscoelasticity of the fluid. Another interesting feature is the increase in the length of the wake in the drag reduction regime: vortex formation occurs at locations that are farther and farther away from the cylinder as Wi increases. These two aspects of the flow structure can be further appreciated through the power spectrum of transverse-velocity variations downstream of the cylinder. Indeed, and as fig. 2d shows, the power spectrum shows a well-defined peak at the shedding frequency for the Newtonian fluid. The height of this peak decreases as the Weissenberg number increases up to its disappearance for $Wi > Wi_2$. We also noted that for the drag reduction regime, the amplitude of the higher harmonics seems to increase with respect to the Newtonian case indicating a large deformation of the wake. Experiments using soap films, for which the flow field is quasi–two-dimensional due to the small thickness of the film, have discussed such an effect as the shedding length increases upon addition of polymer [14]. Here, the shedding length becomes large enough that no shedding is observed in the flow domain used. When this occurs, the drag starts to increase considerably.

Figures 3a and b display a quantitative measurement of the effect of the viscoelasticity. We plot the drag on the cylinder (normalized by the Newtonian drag) for different Reynolds numbers and varying Weissenberg numbers. Two different behaviors are observed as shown in fig. 3a. For $Re < 40$, the drag is similar to that of the Newtonian fluid for small Wi. However, above Wi_2, the drag increases *vs.* Wi. This regime shows the well-known drag enhancement observed in three-dimensional experiments using spheres or cylinders in low Reynolds number flows [6–8], an effect which is well captured by the simulations presented here for the model we have used. The drag is enhanced by a factor which can be as large as 250%. When the Reynolds number is above 40, a different behavior emerges: drag reduction (which can reach 50%) is

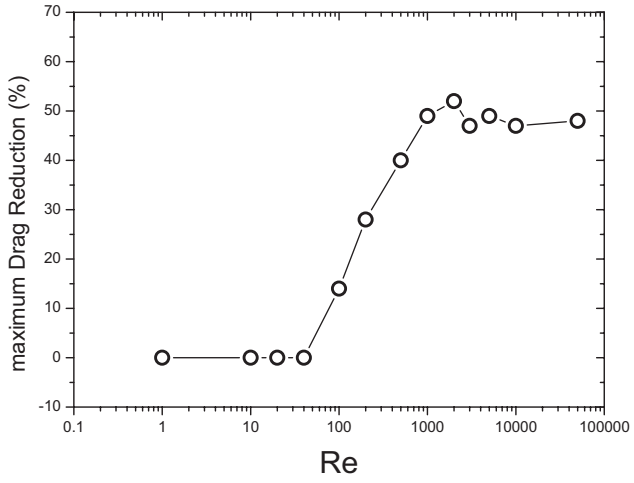

Fig. 4: The percentage of maximum drag reduction *vs.* Reynolds number.

observed above a first threshold value of Wi denoted Wi_1 before the appearance of drag enhancement for $Wi > Wi_2$ (as for the low Re). This behavior is now shown in fig. 3b for all the Reynolds numbers we have examined in this study (except for $Re = 50000$) *vs.* the reduced Weissenberg number (Wi/Wi_2). This figure clearly shows the difference between the low Reynolds numbers for which only drag enhancement is observed for $Wi/Wi_2 > 1$ and the high Reynolds numbers for which drag reduction is observed in an interval of Wi/Wi_2 below 1. The values of the increase in drag do not collapse perfectly for values of the reduced Wi/Wi_2 above 1. For the low Re, the increase is slow at first before a rapid rise while for higher Re, the increase is fast for $Wi/Wi_2 > 1$. The reduction in drag increases as the Reynolds number increases and seems to reach a saturation value for Re near 2000. The drag reduction window (values of Wi for which drag reduction occurs) varies with Re as fig. 1 shows; its extent increases as Re increases before saturating for higher Re. Figure 4 shows the maximum drag reduction *vs.* the Reynolds number and as remarked above, this drag reduction sets in only above $Re = 40$ and increases for values of Re between 40 and 1000 from nearly 0 to 50 percent. This reduction then goes through a mild maximum at $Re = 2000$ before stabilizing on a plateau at about 48%. The location of the maximum drag reduction is reported in fig. 1 as a solid line. This location starts out close to the drag enhancement regime but deviates from it as Re increases and stabilizes at about $\frac{1}{2}Wi_2$.

To further examine the behavior of viscoelastic flow around the cylinder, we plot in fig. 5 the elongation rate $\mathrm{d}u/\mathrm{d}x$, the longitudinal elastic stress σ_{xx}, as well as the pressure variation along the center line of the channel. These quantities change qualitatively as either transition is crossed. We illustrate this behavior using $Re = 10$ and $Re = 100$. For $Re = 10$ and for $Wi < Wi_2$, the elongation rate is close to the Newtonian case. As Wi increases, the location of maximum elongation (which is at 3 radii downstream) migrates towards the cylinder. As Wi increases above Wi_2, the maximum elongation increases and its location migrates towards the cylinder wall. By contrast, for Wi below Wi_2, the elongation rate near the cylinder wall is negative so as the transition from Newtonian drag to enhanced drag is crossed, the elongation near the cylinder wall changes sign. For $Re = 100$, for which three regimes are observed, as Wi_1 is crossed (to the drag reduction zone), the maximum elongation actually decreases and its location migrates away from the cylinder wall. It is only after crossing Wi_2 towards the drag enhancement regime that the maximum elongation starts to increase and its location moves towards the cylinder wall. The signature of either transition is therefore visible in the elongation rate and its variation along the center line.

On the other hand, the maximum of the stress, which occurs near the cylinder wall in the downstream region, increases as Wi increases for $Re = 10$. At the crossing of the transition to drag enhancement, the maximum stress location migrates towards the cylinder wall. That the maximum stress location is at the cylinder wall is true also for $Re = 100$ in the drag enhancement regime. Both the elongation rate and the normal stress are maximal near the cylinder wall for the drag enhancement regime. Experiments in microchannels for small Reynolds numbers in the drag enhancement regime have observed large elongations of the polymers in the vicinity of the cylinder wall on the downstream side [8]. Our simulations seem to capture this essential feature of the experiments despite the fact that our simulations are two dimensional while the experiments are in three dimensions. In the drag reduction regime however, the location of maximum stress and maximum elongation is rather farther away from the cylinder (2.5 cylinder diameters). Another feature associated with the transition from drag enhancement to drag reduction *vs.* Wi can also be appreciated through the variation of the pressure along a cut in the flow direction and in the center line of the channel. The most prominent feature here is the pressure on the downstream side of the cylinder. Note that the pressure first increases with respect to the Newtonian case as the Weissenberg number increases (this is the drag reduction regime) before decreasing to much lower values (with a sharp peak) for Wi greater than Wi_2 indicating a strong increase in the drag on the cylinder. The decrease in pressure is localized near the cylinder wall and its importance increases as Wi increases.

The onset of drag enhancement is therefore accompanied by four distinct features: suppression of vortex shedding for $Re > 40$, a strong positive peak in elongation rate, strong elastic stresses, and a strong dip in pressure near the downstream side of the cylinder. The drag reduction regime is on the other hand accompanied by a rise in pressure, a reduction in elongation rate, but an increase in elastic stresses at a position slightly downstream. These

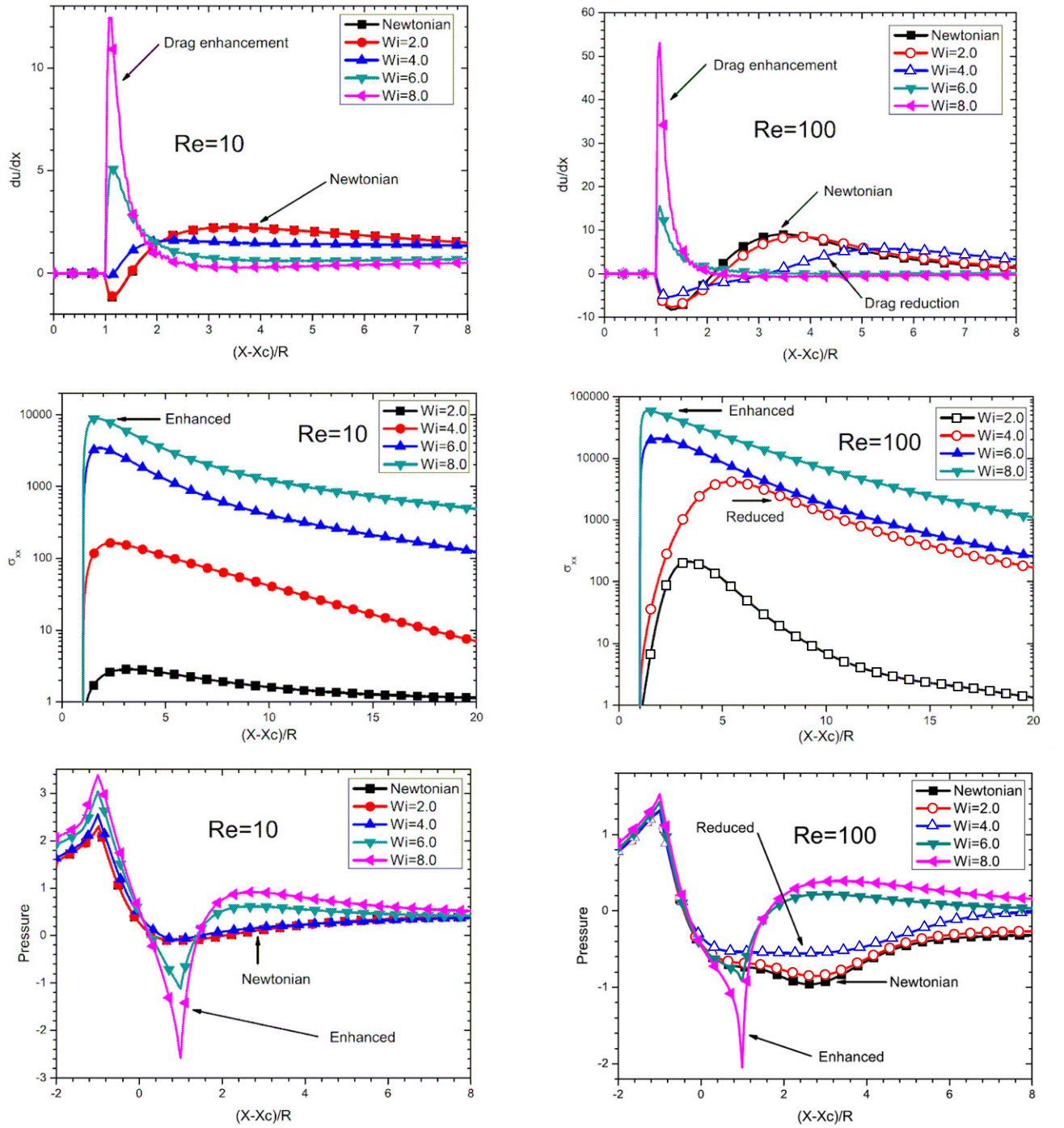

Fig. 5: (Colour on-line) Elongation, longitudinal elastic stress, and pressure variation along the center line of the channel for two different Reynolds numbers and different Wi.

features characterize each regime and point to the importance of what occurs near the downstream stagnation point in determining the drag on the cylinder.

In conclusion, our numerical simulations of the Oldroyd-B model in two dimensions show that drag on a cylinder can be enhanced for low Reynolds numbers but that it can be reduced for higher ones. This behavior is captured in a phase diagram in Reynolds number-Weissenberg number space showing a transition from two to three regimes. The drag enhancement regime at large Reynolds numbers is accompanied by a total suppression of the vortex-shedding instability as well as large elongation rates and a large dip in pressure at the cylinder wall on the downstream side of the cylinder. Despite the limitations

of the model used, several essential features of viscoelastic flow past a cylinder are well captured by the calculations presented here.

REFERENCES

[1] Gyr A. and Bewersdorff H. W., *Drag Reduction of Turbulent Flows by Additives* (Kluwer) 1995.

[2] Tabor M. and De Gennes P. G., *EPL*, **2** (1986) 519.

[3] Sreenivasan K. R. and White C. M., *J. Fluid Mech.*, **409** (2000) 149.

[4] Lvov V. *et al.*, *Phys. Rev. Lett.*, **92** (2004) 244503; Amarouchene Y. *et al.*, *Phys. Fluids*, **20** (2008) 065108.

[5] Brown R. A. and McKinley G. H., *J. Non-Newtonian Fluid Mech.*, **52** (1994) 407.

[6] Chhabra R. P. *et al.*, *Chem. Eng. Soc.*, **56** (2001) 2221.

[7] Verhelst J. M. and Nieuwstadt F. T. M., *J. Non-Newtonian Fluid Mech.*, **116** (2004) 301.

[8] François N. *et al.*, *Phys. Rev. Lett.*, **100** (2008) 018302; François N. *et al.*, *EPL*, **86** (2009) 34002.

[9] Liu A. W. *et al.*, *J. Non-Newtonian Fluid Mech.*, **77** (1998) 153.

[10] Solomon M. J. and Muller S. J., *J. Non-Newtonian Fluid Mech.*, **62** (1996) 81.

[11] Sun J. *et al.*, *J. Non-Newtonian Fluid Mech.*, **86** (1999) 281.

[12] Huang P. Y. and Feng J., *J. Non-Newtonian Fluid Mech.*, **60** (1995) 179.

[13] James D. F., *Annu. Rev. Fluid Mech.*, **41** (2009) 129.

[14] Cressman J. R., Bailey Q. and Goldburg W. I., *Phys. Fluids*, **13** (2002) 867.

[15] Amarouchene Y. and Kellay H., *Phys. Rev. Lett.*, **89** (2002) 104502; Kellay H., *Phys. Rev. E*, **70** (2004) 036310.

[16] Boffetta G. *et al.*, *Phys. Rev. E*, **71** (2005) 036307; Berti S. *et al.*, *Phys. Rev. E*, **77** (2008) 055306.

[17] Angot P. *et al.*, *Numer. Math.*, **81** (1999) 497.

[18] Sureshkumar R. and Beris A. N., *J. Non-Newtonian Fluid Mech.*, **60** (1995) 53.

[19] Bruneau C. H. and Saad M., *Comput. Fluids*, **35** (2006) 326.

[20] Bruneau C. H., Greffier O. and Kellay H., *Phys. Rev. E*, **60** (1999) R1162; Kellay H., Wu X. L. and Goldburg W. I., *Phys. Rev. Lett.*, **74** (1995) 3975; Kellay H., Wu X. L. and Goldburg W. I., *Phys. Rev. Lett.*, **80** (1998) 277; Kellay H., Bruneau C. H. and Wu X. L., *Phys. Rev. Lett.*, **84** (2000) 1696; Bruneau C. H. and Kellay H., *Phys. Rev. E*, **71** (2005) 046305.

[21] Tirtaatmadja V. and Sridhar T., *J. Rheol.*, **39** (1995) 1133.